Thermal conductivity of ceramic/metal composites from preforms produced by freeze casting

D. Hautcoeur, Yannick Lorgouilloux, Anne Leriche, M. Gonon, B. Nait-Ali, D.S. Smith, Véronique Lardot, Francis Cambier

Thermal conductivity of ceramic/metal composites from preforms produced by freeze casting

D. Hautcoeur [a,*], Y. Lorgouilloux [b], A. Leriche [b], M. Gonon [c], B. Nait-Ali [d], D.S. Smith [d], V. Lardot [a], F. Cambier [a]

[a] Belgian Ceramic Research Centre (BCRC), Avenue du Gouverneur Cornez, 4, B-7000 Mons, Belgium
[b] Laboratoire des Matériaux Céramiques et Procédés Associés, Université de Valenciennes et du Hainaut-Cambrésis, Boulevard Charles de Gaulle, 59600 Maubeuge, France
[c] UMONS-FPMs, Pôle Matériaux – Service Science des matériaux, Rue de l'Epargne 56, B-7000 Mons, Belgium
[d] École Nationale Supérieure de Céramique Industrielle, SPCTS, UMR 7315, 12 Rue Atlantis, F-87068 Limoges, France

A B S T R A C T

Porous alumina and zirconia preforms, processed by ice templating, have been used to manufacture ceramic/metal composites by aluminium alloy infiltration. The aim of the present work is to study the influence of the ceramic material nature and of the initial porous structure on the thermal conductivity anisotropy of the composite in order to assess potential applications in the field of thermal management. The materials are characterised in terms of pore volume fraction and pore size before and after metal infiltration. The freeze casted preforms exhibit anisotropic lamellar structures with ellipsoidal pores ranging from 35 μm to 40 μm and porosity fractions from 64 to 67%. After metal infiltration, composite parts present the same anisotropic morphology, which correspond to alternating ceramic and metal layers. Thermal conductivities have been determined, with an average of 80 $W\,m^{-1}\,K^{-1}$ and 13 $W\,m^{-1}\,K^{-1}$ parallel and perpendicular to the freezing direction respectively, for zirconia/metal composites. Theoretical values of thermal conductivity can be calculated using the Maxwell-Eucken relation, to handle the residual porosity, in combination with series and parallel resistance models to describe the overall anisotropic character. These give good agreement to experiment.

Keywords:
Freeze casting
Ice templating
Ceramic/metal composite
Anisotropy
Thermal conductivity

1. Introduction

Porous ceramics are used for diverse applications according to characteristics such as pore volume fraction and distribution, permeability and so on. As examples, porous ceramic structures are used as filters for molten metal [1], water [2] or gas [3] and microfiltration by membranes, but also to process fuel cell electrodes [4], for thermal energy storage devices [5], and for sound [6] or thermal insulation [7]. All these applications are typically developed with isotropic porous materials. In the case of materials exhibiting anisotropic porosity, similar applications are possible, with significant improvements in the properties as it has been demonstrated for the preparation of membranes [8], of piezoelectric substrates [9,10], electrodes for fuel cell (SOFC) [11], biomaterials [12] and ceramic matrix composites [13,14].

Freeze casting by ice templating of ceramic materials, developed in the last 15 years [15], consists of freezing stable ceramic slurry. The porous structure results in the growth of ice crystals and their interaction with the ceramic particles. A green body is then obtained by sublimation of the ice, without shrinkage or damaging the ceramic framework [16]. An anisotropic structure can be produced in specific conditions when the solidification of the slurry is oriented by a thermal gradient [17]. Consequently, the structure presents elongated and continuous pores oriented along the freezing direction. Some authors have shown that these porous materials exhibit anisotropic thermal conductivity [18–20].

An easy way to obtain a ceramic matrix metal composite consists of filling the porosity of a ceramic preform with a metal, by squeeze or die casting [14,21]. In most cases, such composites are made, using an isotropic [22] preforms, but some papers have reported composites prepared from freeze casted ones [23,24]. For example, Roy et al. [14] have filled porous alumina preforms with an aluminium alloy and they studied the elastic behaviour of such composites.

Recently, it has been shown that the orientation of carbon nanofibers in a copper matrix leads to anisotropic thermal conductivity [25]. In such perspective, the present work aims at

* Corresponding author.
E-mail address: d.hautcoeur@bcrc.be (D. Hautcoeur).

investigating the anisotropic thermal conductivity behaviour of ceramic metal composites processed from freeze casted ceramic performs. The structures are characterised in terms of pore volume fraction and pore size before and after metal infiltration. An analytical model is used to calculate values, based on resistances in series and parallel to describe the anisotropic conduction, and the Maxwell-Eucken relation to handle the effect of residual porosity.

2. Experimental procedure

2.1. Materials and methods

Slurries are prepared by mixing 20 vol% of ceramic in deionised water with a small amount of ammonium polymethacrylate anionic dispersant (Dolapix CE64, from Zschimmer and Schwarz, Germany). The ceramic is an alumina powder (d50 ~0.4 μm, specific surface area = 8 $m^2 g^{-1}$, P172SB, Rio Tinto Alcan, Brazil) or a 3 mol% yttria stabilised zirconia powder (d50 ~0.3 μm, specific surface area = 7 $m^2 g^{-1}$, TZ-3YS, Tosoh, Japan). The slurries are then mixed for 24 h in Turbula® with alumina or zirconia beads (diameter of 2 mm). After removing the balls, 3 wt% of polyethylene glycol (Mw = 1000 mol g^{-1}, from Merk, Germany) is added as a binder.

Each slurry is poured into a cylindrical TEFLON mould (30 mm inner diameter and 50 mm high) and put on the freezing device. Fig. 1 illustrates the freeze casting device. The sample holder is cooled slowly down to −40 °C (1 °C/min), and then the temperature is kept constant until the full freezing of the slurry is achieved. The frozen samples are then placed in a freeze dryer (HETO CD8, Thermo Fisher Scientific, USA) for 48 h to remove the solvent at a pressure close to 10 Pa. All green bodies are fired at a constant heating rate of 5 °C/min and maintained during 2 h at 1600 °C (alumina) or 1450 °C (zirconia) and finally cooled down at 5 °C/min to room temperature.

After sintering, ceramic/metal composites are obtained by filling the ceramic preforms with an aluminium alloy, $AlSi_{10}Mg$ (Altara, France) with a purity of 99%, using a vacuum pressure metal casting device (VC-650 V, INDUTHERM, Germany) (Fig. 2). The ceramic part is placed inside a refractory plaster mould which was prepared by investment casting. Aluminium alloy is melted at 740 °C and poured into the mould heated at the same temperature. The mould is then cooled down to ambient temperature naturally. Composites exhibit cylindrical shape with a diameter and a height of about 20 mm. Slices of the composites are cut both perpendicularly and parallel to the freezing direction, to allow the determination of their thermal conductivity at room temperature and examined by SEM and X-ray tomography to evaluate the

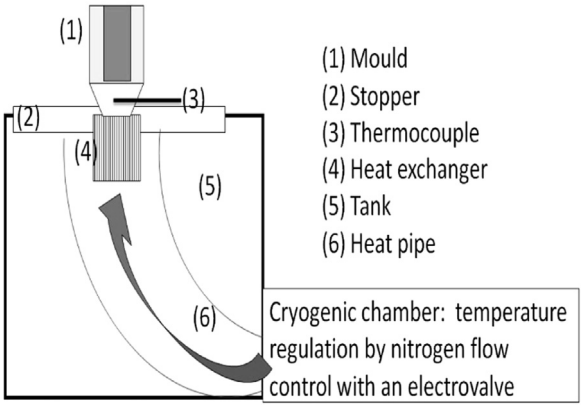

Fig. 1. Schematic representation of the freeze casting device.

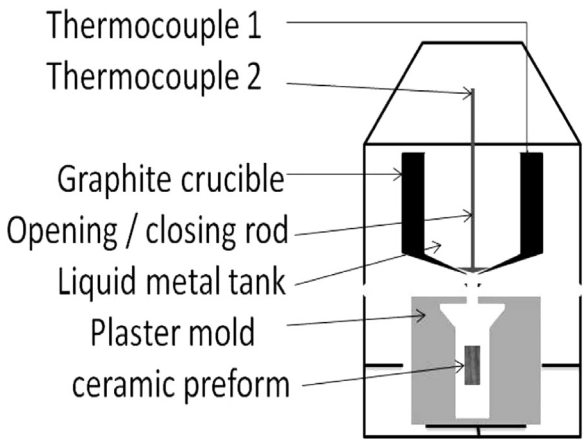

Fig. 2. Schematic representation of the metal infiltration device.

infiltration quality. Typical dimensions of the disk samples are 2 mm in thickness and 14 mm in diameter with parallel and unpolished faces.

2.2. Characterisation

2.2.1. Microstructure

The amount of porosity and bulk density are determined by using the method based on Archimedes' principle for ceramic preforms using deionised water as the liquid medium. Pore size is measured using image analysis of the SEM micrographs (HITACHI S-3500N and JEOL JSM 5900 LV, Japan). For each sample, 10 micrographs with more than 150 pores in total are investigated.

The sintering conditions lead to incomplete densification of the ceramic scaffold, which correspond to the ceramic wall porosity. To determine this micro porosity in the ceramic wall of the porous preforms, an ultrasonic method is used. The measurements are made on cylindrical samples (diameter and height of 20 mm) using two transducers (Ultrasonic tester, Brutsaert, Belgium) with a nominal frequency of 250 kHz, assuming that anisotropic lamellae will act as a waveguide. The transducers are placed on opposite sides of the sample using soft paraffin as a coupling agent.

Calibration curves of wave velocity as a function of porosity are recorded on isotropic alumina and zirconia samples with known porosity amount. These samples are prepared by uniaxial pressing of powder pellets followed by sintering at different temperatures. Three samples were processed for each reference material and the wave velocity is measured six times for each sample. The calibration curves are plotted in Fig. 3. The experimental data are in

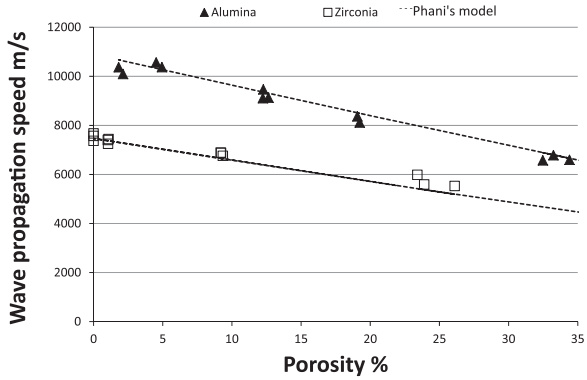

Fig. 3. Standard curves of ultrasound wave propagation speed as a function of porosity for isotropic porous ceramics. Black line correspond to calculated curves from Phani's relation.

good agreement with Phani's relation [26] (Eq. (1)):

$$V_L = V_{L0}(1-p)^m \quad (1)$$

where V and V_{L0} are the wave velocity of the isotropic porous and dense material respectively, p is the pore volume fraction and m is a constant, determined experimentally, with a value of 1.17 for alumina and 1.20 for zirconia.

For the thermal conductivity study, the metal volume fraction is calculated by using Eq. (2):

$$\rho_{composite} = v_{metal}{}^{*}\rho_{metal} + v_{ceramic}{}^{*}\rho_{ceramic} \quad (2)$$

with $\rho_{composite}$, the bulk density of the composite, ρ_{metal} and $\rho_{ceramic}$, the densities of dense aluminium alloy and ceramic respectively, v_{metal} and $v_{ceramic}$ the volume fraction of metal and ceramic, respectively. For this calculation, only the volume fraction of the metal part is unknown (all densities are determined by Archimedes' method). The ceramic volume fraction in the sample is assumed constant before and after metal infiltration. The total pore volume fraction in the composite is then easily deduced using the volume fractions of metal and ceramic (the sum of these three values is one).

2.2.2. Thermal conductivity

Thermal conductivity (λ) is determined by measuring thermal diffusivity (α) using the laser flash method (Netzsch LFA 427, Germany). The flash source is a Nd: YAG laser which delivers pulses at 1.064 μm up to 20J with a typical duration of 500 μs. The sample back face temperature is monitored with a liquid-nitrogen-cooled infra-red detector (InSb). To improve the laser beam absorption and the emitted signal from the back face, samples are coated with a thin graphite layer by spray coating and each disk is tested 5 times. Cape and Lehman's model which takes into account heat losses during the experiment, was used to calculate the thermal diffusivity (α) [27]. The thermal conductivity is calculated using the Eq.3.:

$$\lambda = \alpha\, \rho\, C_p \quad (3)$$

where ρ is the bulk density and C_p is the specific heat of the material which was calculated for each composite using the rule of mixture. Literature values used for alumina and zirconia respectively are 770 J Kg^{-1} K^{-1} and 456 J Kg^{-1} K^{-1} [28]. For the metal alloy, the specific heat value of 900 J Kg^{-1} K^{-1} was given by the supplier is used.

Thermal diffusivity is measured on disks cut in two directions, parallel and perpendicular to the ice front formation, in the same sample. The resulting thermal conductivity values are denoted $\lambda_{parallel}$ and $\lambda_{perpendicular}$. The ratio $\frac{\lambda_{parallel}}{\lambda_{perpendicular}}$ was calculated to evaluate "the thermal conductivity anisotropy". In order to employ two-phase analytical relations, measurements were also performed on almost fully dense alumina, zirconia and on the alloy.

3. Results and discussion

3.1. Structure

3.1.1. Porous preforms

SEM micrographs of Fig. 4 correspond to a cross section parallel to the freezing direction. At the bottom part of the sample, in both cases, a denser zone with a different morphology (Fig. 4b), inherent to the process of ice templating is observed. These zones have been removed before ceramic scaffold characterisation (porosity level and pore size) and before the metal infiltration. As described in literature [29], the presence of this heterogeneous zone can be explained by a fast stable freezing front during the first instants of the freezing.

Table 1 shows the main characteristics of the porous samples (preforms in alumina: AlP, or in zirconia: ZrP), before metal infiltration. The structure of the porous preform is a classic lamellar morphology characterised by ceramic walls with thickness between 30 and 40 μm.

Elliptic pore shape is observed, which is characteristic of freeze casting by ice templating [30], as can be seen in Fig. 5. Owing to the standard deviation, both the small (a) or larger (b) diameter can be consider equivalent for both types of ceramics as shown the SEM micrographs (Fig. 5(a) and (b), Table 1). They only differ in terms of total porosity, slightly higher for alumina sample (less than 3%). The sample porosity corresponds to the ice sublimation during the freeze drying step. In both cases, a 20% vol. slurry solid content was chosen to promote a high amount of porosity in order to allow an easier metal infiltration of the ceramic preforms. The micro porosity, determined by the acoustic test, is similar for both alumina and zirconia.

3.1.2. Composites

Composite structures are observed in both directions of orientation on samples prepared for thermal diffusivity measurements. The observations in the direction parallel to that of freezing direction allow the state of the ceramic – metal interface to be examined and in the perpendicular direction to visualize infiltration defects. The analyses were performed by SEM and by X-ray radiography for alumina and zirconia – metal composites. Similar results are obtained in both cases, only the zirconia – metal composites were described.

Figs. 6 and 7 show the SEM micrographs of zirconia/metal

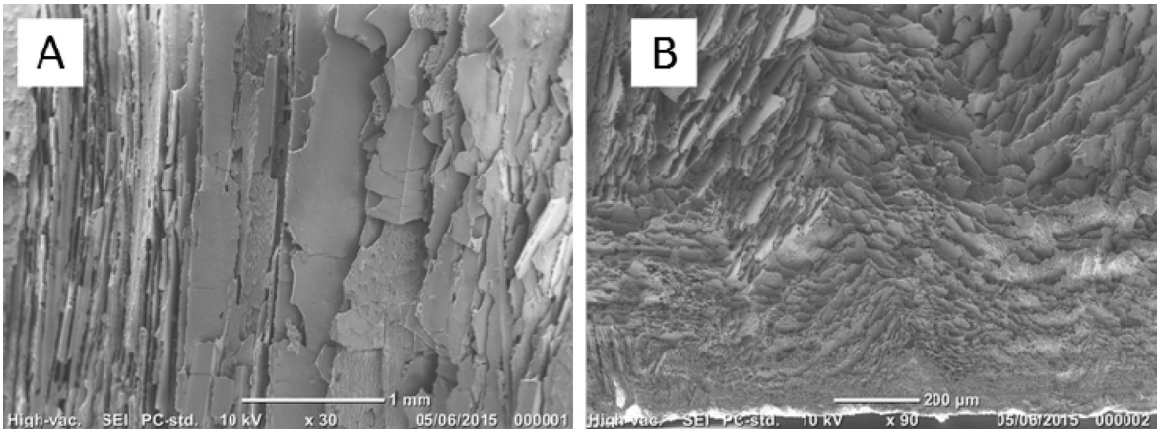

Fig. 4. SEM images of zirconia at the center (A) and at the bottom (B) sample cross section parallel to the freezing direction.

Table 1.
Pore size and total porosity of alumina and zirconia freeze casted preforms. (a and b are the short and large axis of the ellipsoidal pore respectively).

Samples	Pore size "a" (μm)	Pore size "b" (μm)	Total porosity (%)	Micro-porosity (%)
AlP	35 ± 8	230 ± 100	67.0 ± 1.0	9 ± 1
ZrP	40 ± 8	250 ± 80	64.2 ± 0.3	10 ± 1

composites in the parallel direction to the freezing direction. The dark phase corresponds to metal and the light one is the ceramic. The entire macro porosity, from ice sublimation, appears to be fully infiltrated by the metal despite the surface irregularities of the ceramic walls as shown in Fig. 6b. At low magnification (Fig. 7a), an overall view of sample surface is observed. Some unfilled zones were detected, which are mostly due to the grinding of sample surface. But, by looking closely at the ceramic/metal interface, other defects are identified as shown in Fig. 7b. These black holes might correspond to a remaining closed porosity.

The metal infiltration does not affect the integrity of the ceramic walls since no broken walls are observed as shown in Fig. 8. However, a small number of not fully infiltrated pores are observed (Fig. 8 white arrows). In order to identify if pores are due to the preparation of the sample, X-ray radiography was performed.

Radiographs were taken on flat disk samples (the same as those used for thermal diffusivity measurements). Fig. 9 represents the grey level images taken at 0° and 45° for cuts perpendicular and parallel to the freezing direction. In the case of the perpendicular analysis (Fig. 9a and b), very few holes are observed (black points indicated by black arrows) whatever the sample angle position. It means that, for disks with a 2 mm thickness, the porosity should not be due to surface machining. These pores correspond to metal infiltration defects. Moreover, radiographs made at 45° confirm that these pores are continuous along the whole thickness. In the other direction (parallel to the freezing direction), no see-through porosity was observed. However, some dark grey rich regions were observed which implies the presence of density variation or closed porosity (Fig. 9c black arrows) at an angle of 0°. Furthermore, the sample rotation of 45° reveals the surface roughness to be observed (Fig. 9d black arrows) which appears to be quite high. These observations confirm that closed porosity is present inside the ceramic/metal composite, but only along the infiltration direction, which correspond to macroscopic pore orientation (freezing direction).

3.2. *Thermal conductivity study*

The density and the thermal conductivity of the two dense ceramics and of the alloy were determined. The dense aluminium alloy came from a metal part remaining around the composite after the metal infiltration step. Experimental values obtained for bulk density and thermal conductivity, calculated from measured thermal diffusivity, on dense ceramics and alloy samples, are given in Table 2. Values for alumina and for zirconia are in good agreement with literature data [31,32].

Table 3 gives the results of all volume fractions for the alumina and zirconia composites. Based on these phase proportions, thermal conductivities were calculated from thermal diffusivity measurements. Results are represented in Fig. 10. Some dispersion in thermal conductivities values was observed, especially for zirconia composites in the parallel direction.

For alumina composites, thermal conductivities range from 98 to 114 $W\,m^{-1}\,K^{-1}$ and from 41 to 78 $W\,m^{-1}\,K^{-1}$ parallel and perpendicular to the freezing direction, respectively. Considering the average of experimental values in both directions, an anisotropic thermal conductivity factor of 1.8 was estimated.

Zirconia exhibits a lower thermal conductivity than alumina. Consequently, the mean anisotropic factor of zirconia composites increases from 1.8 to 6.4. Indeed, zirconia composites exhibit a thermal conductivity ranging from 59.4 to 93 $W\,m^{-1}\,K^{-1}$ and from 7.4 to 26.6 $W\,m^{-1}\,K^{-1}$ parallel and perpendicular to the freezing direction, respectively. The maximum measured anisotropy ratios were 2.3 and 11.4 for alumina and zirconia composites, respectively. This difference of a factor of 5 is quite low considering the thermal conductivity of both dense alumina and zirconia where the ratio is about 12.5.

4. Prediction with analytical relations

Many analytical models exist to describe the thermal conductivity of multiphase materials. In each model, assumptions are made on the geometrical arrangement of the different phases. The series and parallel resistances models give the upper and lower limit of the effective thermal conductivity calculated respectively with:

$$\lambda_{eff,series} = \left(\sum_i \frac{v_i}{\lambda_i} \right)^{-1} \tag{4}$$

$$\lambda_{eff,parallel} = \sum_i \lambda_i v_i \tag{5}$$

Our composite materials are constituted of three phases: the ceramic, the metal and air, with volume fractions (v_i) given in Table 3. The microstructure exhibit solid lamellae strongly oriented, in the direction parallel to the ice formation. We have first compared the experimental results with predictions made with the models of series and parallel resistors as shown in Fig. 11.

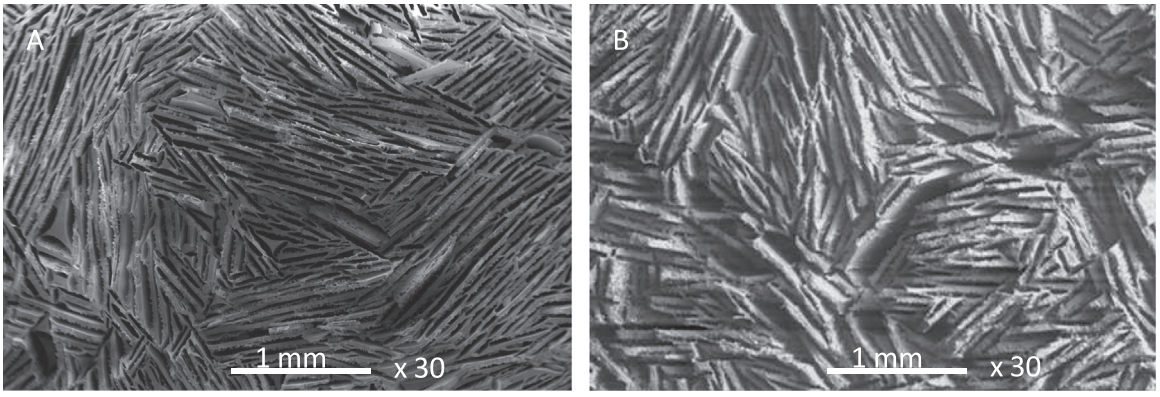

Fig. 5. SEM images of zirconia (A) and alumina (B) sample cross section perpendicular to the freezing direction.

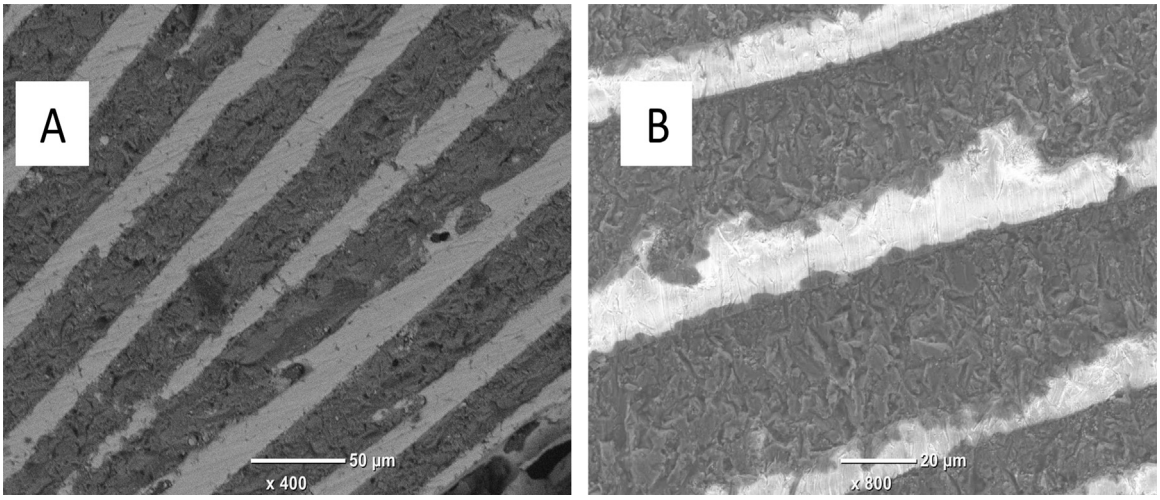

Fig. 6. SEM images of zirconia/metal composite sample cross section parallel to the freezing direction.

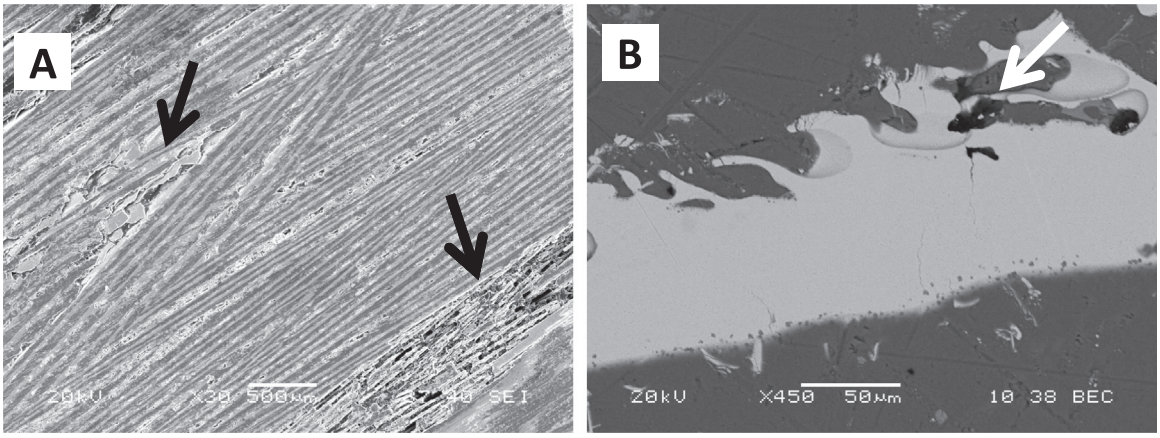

Fig. 7. SEM images of zirconia/metal composite sample cross section parallel to the freezing direction showing the defects.

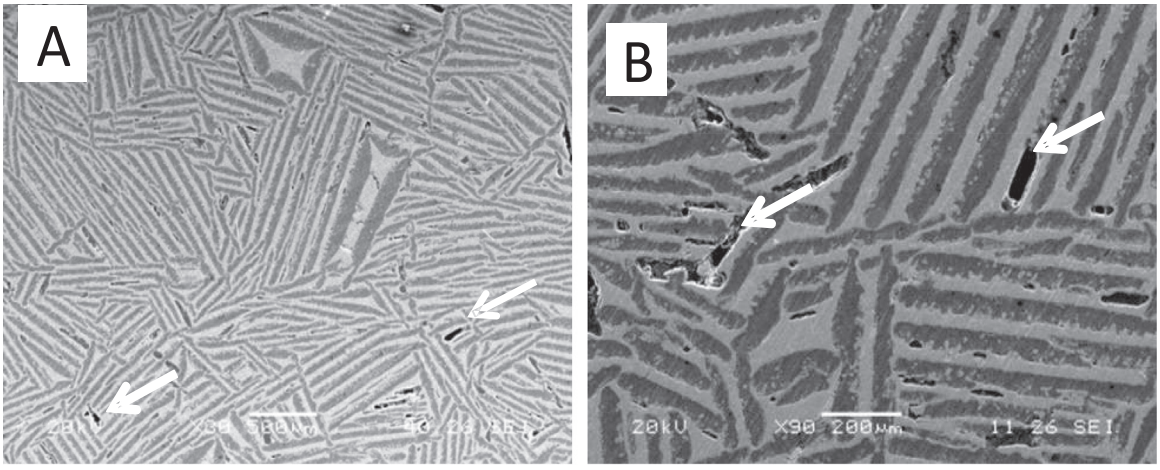

Fig. 8. SEM images of zirconia/metal composite sample cross section perpendicular to the freezing direction.

In the freezing direction, the parallel resistance model predicts relatively the correct trend with a maximum deviation of about 10 $W\,m^{-1}\,K^{-1}$ to experimental values. On the contrary, in the case of the perpendicular orientation, the series analytical model is totally unsuitable. This difference can be explained by the very low thermal conductivity of air. Indeed, with this analytical model, the residual porosity is considered as a continuous insulating phase and hence blocking to the heat flow.

So, this results obtained in the case of perpendicular direction is explained by a wrong geometry arrangement of the residual porosity and another distribution of the porosity has to be assumed for a better prediction, based on isolated spherical inclusion in a continuous matrix (the ceramic/metal composite) as described in Fig. 12.

In that case, the Maxwell-Eucken relation can be used [33,34]. This simplification of the microstructure corresponds, for example,

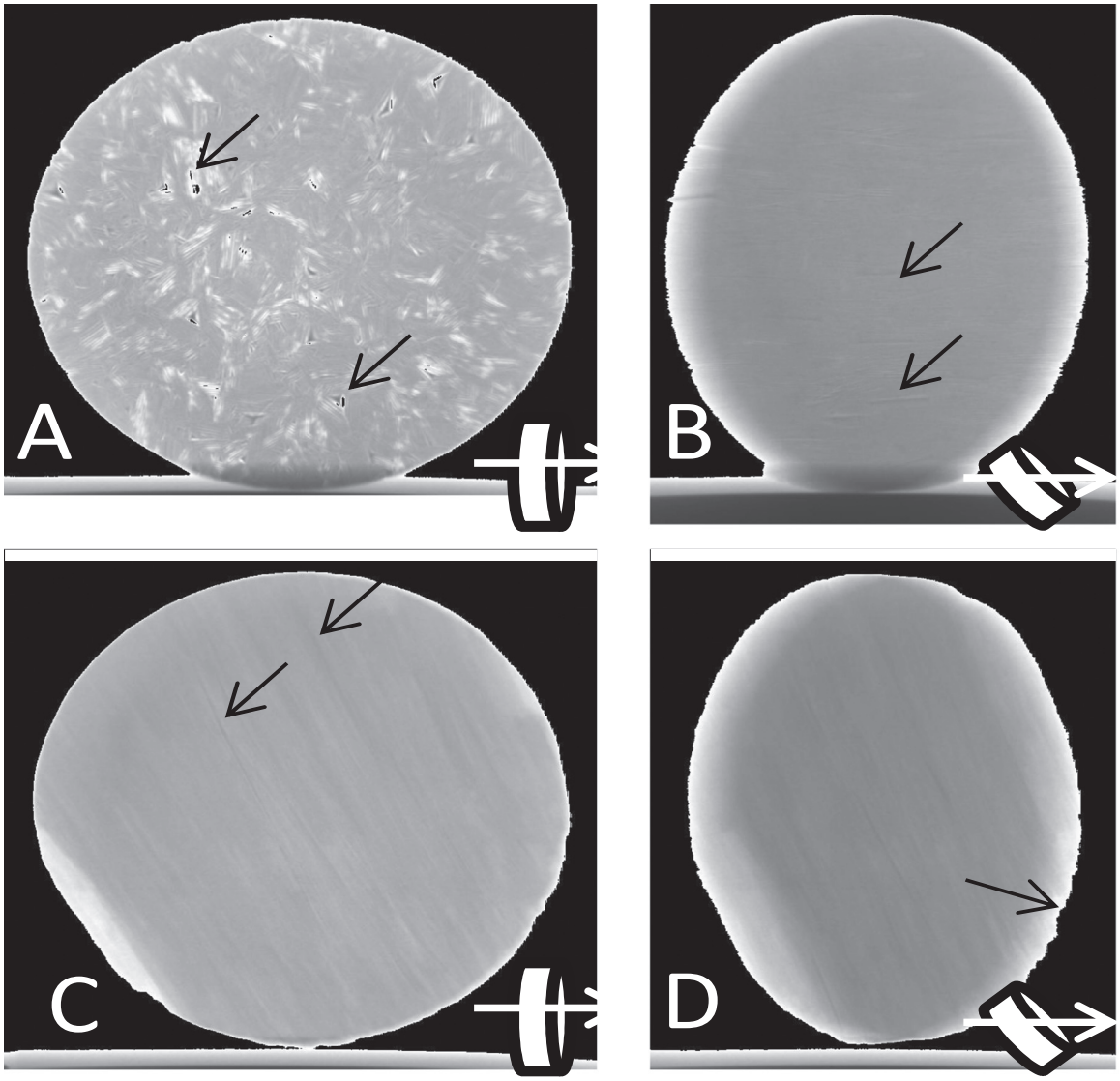

Fig. 9. X-Ray radiography images of zirconia/metal composite sample cross section parallel (a and b) and perpendicular (b and c) to the freezing direction. Image a and c at 0° angle and b and d at 45°.

Table 2.
Experimental characteristics of dense material used for the process of the ceramic/metal composites.

Material	Density (g cm^{-3})	Thermal conductivity (W m^{-1} K^{-1})
Aluminium alloy	2.64	180
Alumina	3.97	35
Zirconia	6.05	2.8

to porous materials with closed pores and the effective thermal conductivity can be calculated with:

$$\lambda_{eff} = \lambda_s \frac{\lambda_p + 2\lambda_s + 2v_p(\lambda_p - \lambda_s)}{\lambda_p + 2\lambda_s - v_p(\lambda_p - \lambda_s)} \quad (6)$$

where λ_s is the thermal conductivity of the solid phase, λ_p and v_p are the thermal conductivity and the volume fraction of the porosity.

To improve the analytical predictions, we propose, according to the microstructure, a three step calculation. The first step uses Eq. (6) to take into account the influence of the residual porosity in the ceramic phase, determined by using the ultrasonic technique described before (Fig. 3). These values correspond to the maximum amount of porosity that can be present in the ceramic wall after metal infiltration. Higher residual porosity means that the porosity is located outside the ceramic phase, in the metal phase or at the ceramic/metal interface, with no preferential location.

The second step of the calculation consists of applying an approach based on a series or parallel arrangement of resistors ((Eqs. (4) and 5)). The calculation was made using the metal thermal conductivity and the ceramic wall thermal conductivity (obtained at the first step). Assuming that the remaining porosity is not inside the ceramic phase, the excess of porosity has to be placed, as closed porosity, in the complete composites. This is the last calculation step where Eq. (6). is used again with the thermal conductivity obtained by second step calculation as input. At each step of the calculation, the volume fractions of every phase were recalculated.

Tables 4 and 5 give the calculated values obtained for alumina and zirconia composites parallel and perpendicular to the freezing direction respectively, in comparison to the experimental values. These results are also plotted in Fig. 11. In the case of the thermal conductivity parallel to the freezing direction, a relatively small difference is observed between calculated values and

Table 3.
Summary of the ceramic, metal and porosity volume fraction for composite samples.

	In parallel direction				In perpendicular direction			
Material	Sample	Metal (vol%)	Ceramic (vol%)	Porosity (vol%)	Sample	Metal (vol%)	Ceramic (vol%)	Porosity (vol%)
Alumina composites	Para Al 1	57.4	31.5	11.1	Perp Al 1	56.3	31.5	12.2
	Para Al 2	58.6	31.5	9.9	Perp Al 2	54.2	31.5	14.3
	Para Al 3	56.2	32.1	11.7	Perp Al 3	57	32.1	10.9
	Para Al 4	54.4	32.1	13.5	Perp Al 4	56.4	32.1	11.5
	Para Al 5	53.4	33.6	13	Perp Al 5	55.3	33.6	11.1
	Para Al 6	55.7	34.5	9.8	Perp Al 6	55.3	33.6	11.1
	Para Al 7	57.8	34.5	7.7	Perp Al 7	57	33.6	9.4
	Para Al 8	56.8	34.5	8.7	Perp Al 8	55.5	33.6	10.9
Zirconia composites	Para Zr 1	57.8	35.7	6.5	Perp Zr 1	45.6	35.7	18.7
	Para Zr 2	43	35.7	21.3	Perp Zr 2	38.4	35.7	25.9
	Para Zr 3	58.9	35.7	5.4	Perp Zr 3	38.7	36	25.3
	Para Zr 4	31.6	35.7	32.7	Perp Zr 4	39.2	36	24.8
	Para Zr 5	42.3	36.5	21.2	Perp Zr 5	39.8	36	24.2
	Para Zr 6	51.9	36.5	11.6	Perp Zr 6	45.6	36	18.4

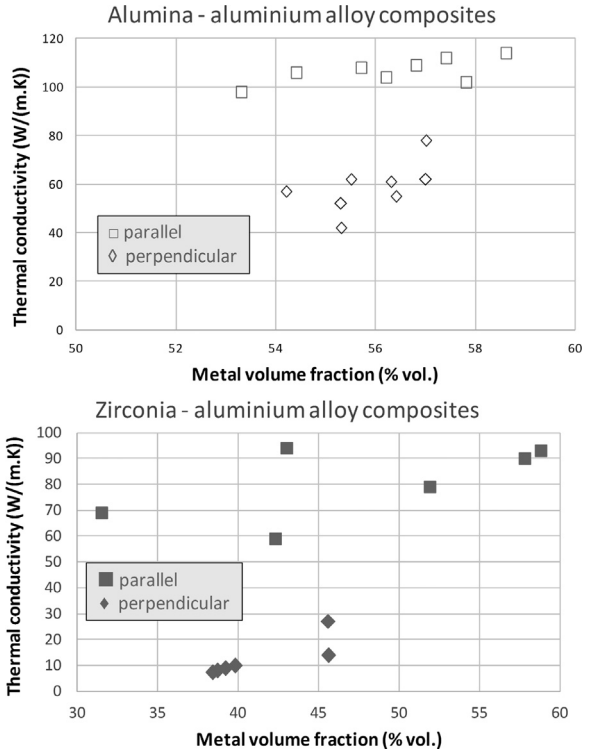

Fig. 10. Graphic representations of composite thermal conductivities as a function of metal volume fraction for alumina metal composite and zirconia for parallel and for perpendicular direction.

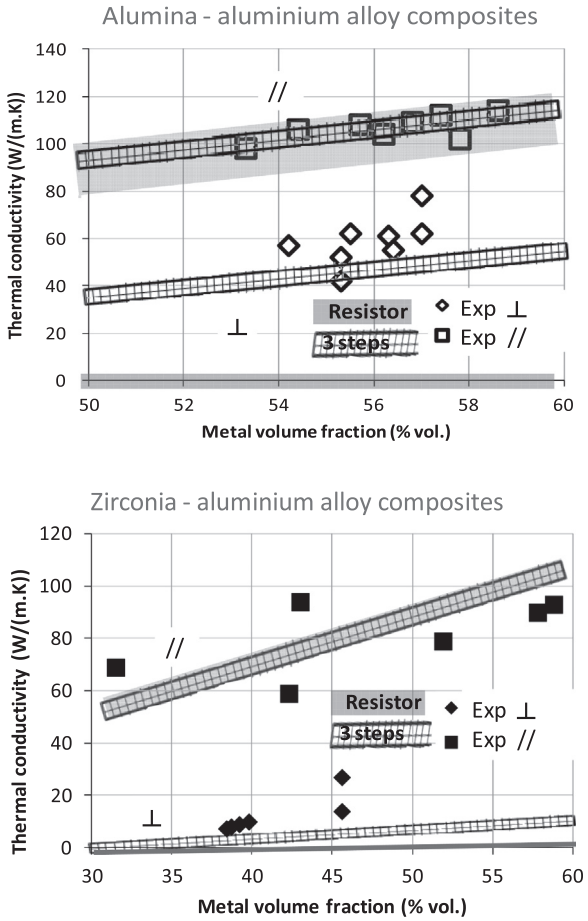

Fig. 11. graphic representations of composite thermal conductivities as a function of metal volume fraction for alumina and zirconia metal composite calculated using series and parallel resistor law (grey zones) and the 3 steps calculation (cross-hatched black zones).

experimental ones, as it is also the case with the model of parallel resistances. As described before, a denser part at the bottom of the sample is always observed due to sedimentation during the freezing step or with the fast freezing front during the first moments of the freezing step. This phenomenon may lead to the formation of a porosity gradient along the freeze cast preform axis. Moreover, in order to make more measurements, several disks were cut inside the same sample after metal infiltration. For the calculation of the metal fraction, an identical ceramic fraction was assumed for all disks. However, this assumption of identical ceramic fraction introduces a calculation error for the metal fraction for the disk because of the porosity gradient.

So, on the one hand, when the calculation predicts a higher thermal conductivity than experimental values, it may be directly linked to error in the pore volume fraction value. On the other hand, when the experimental values are higher, it can only be explained by an inaccurate determination of ceramic/metal volume fractions due to the porosity gradient of the ceramic preform.

To confirm this, average values were estimated for the calculated and experimental ones meaning that any porosity gradient has been compensated. In the case of alumina composite, average values of 110 $W\,m^{-1}\,K^{-1}$ and 106 $W\,m^{-1}\,K^{-1}$ were obtained for the calculated and experimental thermal conductivities,

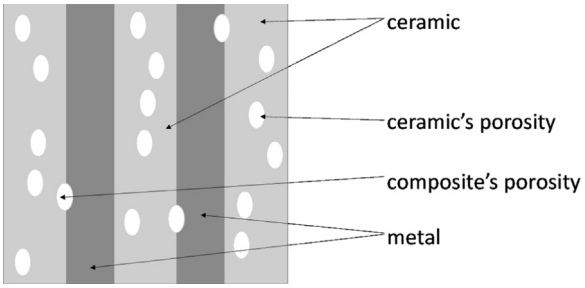

Fig. 12. Schematic representation of porosity repartition for the model calculation.

Table 4.
Comparison of experimental and calculated thermal conductivity for alumina and zirconia composite in the parallel direction.

Material	Parallel	Calculated thermal conductivity ($W\,m^{-1}\,K^{-1}$)	Experimental thermal conductivity ($W\,m^{-1}\,K^{-1}$)
Alumina composites	Para Al 1	112	112 ± 3
	Para Al 2	114	114 ± 3
	Para Al 3	109	104 ± 3
	Para Al 4	104	106 ± 3
	Para Al 5	104	98 ± 3
	Para Al 6	111	108 ± 3
	Para Al 7	115	102 ± 3
	Para Al 8	113	109 ± 3
Zirconia composites	Para Zr 1	105	90 ± 3
	Para Zr 2	74	94 ± 3
	Para Zr 3	107	93 ± 3
	Para Zr 4	52	69 ± 2
	Para Zr 5	73	59 ± 2
	Para Zr 6	93	79 ± 2

Table 5.
Comparison of experimental and calculated thermal conductivity for alumina and zirconia composite in the perpendicular direction.

Material	Perpendicular	Calculated thermal conductivity ($W\,m^{-1}\,K^{-1}$)	Experimental thermal conductivity ($W\,m^{-1}\,K^{-1}$)
Alumina composites	Perp Al 1	48	61 ± 2
	Perp Al 2	46	57 ± 2
	Perp Al 3	50	62 ± 2
	Perp Al 4	49	55 ± 2
	Perp Al 5	46	42 ± 1
	Perp Al 6	46	52 ± 2
	Perp Al 7	49	78 ± 3
	Perp Al 8	47	62 ± 2
Zirconia composites	Perp Zr 1	3,4	26.6 ± 0.4
	Perp Zr 2	2,8	7.4 ± 0.2
	Perp Zr 3	2,8	8.1 ± 0.2
	Perp Zr 4	2,8	9.0 ± 0.3
	Perp Zr 5	2,9	10 ± 0.3
	Perp Zr 6	3,3	14 ± 0.4

respectively. In this case, a good match is observed. For zirconia composite, the trend is similar with an average calculated value of $84\,W\,m^{-1}\,K^{-1}$ and an average experimental one of $80\,W\,m^{-1}\,K^{-1}$. These results confirm that the model can predict correctly the thermal conductivity for a sample if the ceramic fraction before metal infiltration has been determined accurately.

For disks cut perpendicular to the freezing direction, whatever the ceramic nature, the experimental values are higher than the calculated values (except for one sample). Obviously, this deviation may be linked to the same behaviour as observed in the case of parallel disks with the assumption of a constant ceramic volume fraction. However, it was observed by SEM that the pores are randomly oriented along the x,y plan (z axis is the sample height). Indeed, for disks cut in parallel direction, pores in ceramic preform are oriented in the same direction, but in the perpendicular direction, pores are not organised in the same direction. This means that the samples are not perfectly oriented as assumed in the series model used for the calculation step 2. It would be better to consider another parallel contribution which will lead to an increase of the theoretical value. Nevertheless, the proposed analytical calculation gives a lower limit for the thermal conductivity which is closer to experimental results than the only use of Eq. (4).

5. Conclusion

Ceramic freeze cast preforms were used to process ceramic based metal composites by the infiltration of porosity by an aluminium alloy. Ceramic preforms exhibit an overall porosity of about 65% and a pore size of 40 μm and 250 μm for the small and large diameter (ellipsoidal shape). The porosity structure is a direct replica of the grown ice crystals during the freezing step. The structure is anisotropic with a lamellar morphology.

The addition of the metal inside the sample does not damage the overall structure. Anisotropy is maintained, but there is the formation of a few defects as detected by X-ray tomography and SEM observations. To quantify the thermal conductivity anisotropy of the composites, samples were cut perpendicular and parallel to the lamellar orientation (*i.e.* freezing direction). We observed that for a greater difference in the metal and ceramic conductivity values, the thermal anisotropy is revealed. The average thermal conductivity anisotropy ratios are for alumina composite is 1.8, and for zirconia composite 6.4. A maximum value of 11.4 in the case of zirconia/metal composites was achieved.

An original model based on Maxwell-Eucken relation and series/parallel resistor networks was used to predict the thermal conductivity. The comparison of calculated and experimental values showed the influence of the preform micro porosity and structure on the predicted values. The assumption made on the ceramic volume fraction has an important impact on the calculated metal volume fraction and therefore calculated thermal conductivity. Indeed, in the parallel direction, as the orientation of each phase is the same, the difference between experimental and calculated values is explained by difference between real and estimated phase fractions. In the perpendicular direction, it is shown that the non perfect orientation of each phase may explain the differences between experimental and calculated thermal conductivity.

Acknowledgements

We acknowledge the FSE and the DGO6 of the "Service public de Wallonie" for their financial support (grant number ECV320600FDOO7F/1017208/ECOPOR).

References

[1] L.J. Gauckler, M.M. Waeber, C. Conti, M. Jacob-Duliere, Ceramic foam for molten metal filtration, J. Met. 37 (9) (1985) p47–p50.
[2] Z. Xing, J. Li, Q. Wang, W. Zhou, G. Tian, K. Pan, C. Tian, J. Zou, H. Fu, A floating porous crystalline TiO_2 ceramic with enhanced photocatalytic performance for wastewater decontamination, Eur. J. Inorg. Chem. (2013) 2411–2417.
[3] S. Kitaoka, Y. Matsushima, Thermal cyclic fatigue behavior of porous ceramics for gas cleaning, J. Am. Ceram. Soc. 95 (2) (2012) p799–p804.
[4] F. Climent, R. Capellades, J. Gil, E. Garcia, Study of the impregnation of porous anodes of tantalum capacitors with liquids, J. Colloid Interface Sci. 128 (2) (1989) p320–p327.
[5] T. Nomura, N. Okinaka, T. Akiyama, Impregnation of porous material with

phase change material for thermal energy storage, Mater. Chem. Phys. 115 (2009) p846–p850.
[6] M. Carlesso, R. Giacomelli, S. Günther, D. Koch, S. Kroll, S. Odenbach, K. Rezwan, Near-net-shaped porous ceramics for potential sound absorption applications at high temperatures, J. Am. Ceram. Soc. 96 (3) (2013) p710–p718.
[7] R.J. Goldstein, W.E. Ibele, S.V. Patankar, T.W. Simon, T.H. Kuehn, P.J. Strykowski, K.K. Tamma, J.V.R. Heberlein, J.H. Davidson, J. Bischof, F.A. Kulacki, U. Kortshagen, S. Garrick, V. Srinivasan, K. Ghosh, R. Mittal, Heat transfer—A review of 2004 literature, International Journal of Heat and Mass Transfer, 53, 2010, pp. 4343–4396.
[8] M.K. Lee, N.-O. Chung, J. Lee, Membranes with through-thickness porosity prepared by unidirectional freezing, Polymer 51 (2010) p6258–p6267.
[9] S.-H. Lee, S.-H. Jun, H.-E. Kim, Piezoelectric properties of PZT-based ceramic with highly aligned pores, J. Am. Ceram. Soc. 91 (6) (2008) p1912–p1915.
[10] R. Guo, C.-A. Wang, A. Yang, Effects of pore size and orientation on dielectric and piezoelectric properties of 1–3 type porous PZT ceramics, J. Eur. Ceram. Soc. 31 (2011) p605–p609.
[11] Y. Chen, J. Bunch, T. Li, Z. Mao, F. Chen, Novel functionally graded acicular electrode for solid oxide cells fabricated by the freeze-tape-casting process, J. Power Sources 213 (2012) p93–p99.
[12] A. Szepes, J. Ulrich, Z. Farkas, J. Kovacs, P. Szabo-Resez, Freeze-casting technique in the development of solid drug delivery systems, Chem. Eng. Process. 46 (2007) p230–p238.
[13] D.C. Phillips, Ceramic composites: their current status and some requirements for future development, Compos. Sci. Technol. 40 (1991) 1–17.
[14] Siddhartha Roy, Alexander Wanner, Metal/ceramic composites from freeze-cast ceramic preforms: domain structure and elastic properties, Compos. Sci. Technol. 68 (2008) 1136–1143.
[15] T. Fukasawa, Z.-Y. Deng, M. Ando, Pore structure of porous ceramics synthesized from water-based slurry by freeze-dry process, J. Mater. Sci. 36 (2001) 2523–2527.
[16] S. Deville, Freeze casting of porous ceramics: a review of current achievements and issues, Adv. Eng. Mater. 10 (3) (2008) 155–169.
[17] T. Waschkies, R. Oberacker, M.J. Hoffmann, Control of lamellae spacing during freeze casting of ceramics using double-side cooling as a novel processing route, J. Am. Ceram. Soc. 92 (S1) (2006) S79–S84.
[18] S.R. Hostler, A.R. Abramson, M.D. Gawryla, S.A. Bandi, D.A. Schiraldi, Thermal conductivity of a clay-based aerogel, Int. J. Heat. Mass. Transf. 52 (2009) 665–669.
[19] F. Bouville, E. Maire, S. Deville, Self-assembly of faceted particles triggered by a moving ice front, Langmuir 30 (2014) 8656–8663.
[20] A. De Marcos, B. Nait-Ali, N. Tessier-Doyen, A. Alzina, C. Pagnoux, C. S. Peyratout, Influence of the ice front velocity and of the composition of suspensions on thermal properties of bentonite materials prepared using freeze-casting process, J. Eur. Ceram. Soc. 34 (2014) 4433–4441.
[21] K. Naplocha, A. Janus, J.W. Kaczmar, Z. Samsonowicz, Technology and mechanical properties of ceramic preforms for composite materials, J. Mater. Process. Technol. 106 (2000) 119–122.
[22] M. Nakata, K. Suganuma, Effect of internal structure on thermal properties of alumina/aluminum composites fabricated by gelate-freezing and partial-sintering process, respectively, Mater. Trans. 46 (1) (2005) 130–135.
[23] T. Ziegler, A. Neubrand, S. Roy, A. Wanner, R. Piat, Elastic constants of metal/ceramic composites with lamellar microstructures: finite element modelling and ultrasonic experiments, Compos. Sci. Technol. 69 (2009) 620–626.
[24] T. Ziegler, A. Neubrand, R. Piat, Multiscale homogenization models for the elastic behaviour of metal/ceramic composites with lamellar domains, Compos. Sci. Technol. 70 (2010) 664–670.
[25] D. Marcos-Gómez, J. Ching-Lloyd, M.R. Elizalde, W.J. Clegg, J.M. Molina-Aldareguia, Predicting the thermal conductivity of composite materials with imperfect interfaces, Compos. Sci. Technol. 70 (2010) 2276–2283.
[26] M. Asmani, C. Kermel, A. Leriche, M. Ourak, Influence of porosity on Young's modulus and Poisson's ratio in alumina ceramics, J. Eur. Ceram. Soc. 21 (2001) p1081–p1086.
[27] J.A. Cape, G.W. Lehman, Temperature and finite pulse-time effects in the flash method for measuring thermal diffusivity, J. Appl. Phys. 34 (1963) p1909–p1913.
[28] O. Knacke, O. Kubaschewski, K. Hesselmann, Thermochemical Properties of Inorganic Substances, Second edition, Springer-Verlag,, 1991.
[29] S. Deville, E. Maire, A. Lasalle, A. Bogner, C. Gauthier, J. Leloup, C. Guizard, Mmetastable and unstable cellular solidification of colloidal suspensions, Nat. Mater. 8 (2009) 966–974.
[30] S. Deville, E. Saiz, A.P. Tomsia, Ice-templated porous alumina structures, Acta Mater. 55 (2007) 1965–1974.
[31] S. Raghavan, H. Wang, R.B. Dinwiddie, W.D. Porter, M.J. Mayo, The effect of grain size, porosity and yttria content on the thermal conductivity of nanocrystalline zirconia, Scr. Mater. 39 (1998) p1119–p1125.
[32] P.A. Popov, V.D. Solomennik, P.V. Belyaev, L.A. Lytvynov, V.M. Puzikov, Thermal conductivity of pure and Cr^{3+} and Ti^{3+} doped Al_2O_3 crystals in 50–300 K temperature range, Funct. Mater. 18 (2011) p476–p480.
[33] J. Maxwell, A treatise on Electricity and Magnetism, Clarendon Press, Oxford, 1892.
[34] D.S. Smith, A. Alzina, J. Bourret, B. Nait-Ali, F. Pennec, N. Tessier-Doyen, K. Otsu, H. Matsubara, P. Elser, U.T. Gonzenbach, Thermal conductivity of porous materials, J. Mater. Res. 28 (2013) p2260–p2272.